BACHELOR THESIS

TRANSCUTANEOUS ELECTRICAL STIMULATION MODULATES PERSISTENT INWARD CURRENTS IN SPINAL CORD INJURY SUBJECTS: A MODEL-BASED STUDY

O.I. Zantingh

FACTULTY OF ENGINEERING TECHNOLOGY
DEPARTMENT OF BIOMECHANICAL ENGINEERING

EXAMINATION COMMITTEE
Prof. dr. ir. M. Sartori
R.E. Ornelas Kobayashi, MSc.
dr. S.U. Yavuz

DOCUMENT NUMBER
BE - 948

UNIVERSITY OF TWENTE.

29/08/2023

ABSTRACT

Spasticity is a highly prevalent motor-impaired condition among spinal cord injury patients and stroke survivors. Transcutaneous spinal direct current stimulation (tsDCS) aims to improve the modulation of spinal excitability in individuals with spasticity. Multiple mechanisms may play a role in spinal excitability regulation in spastic patients, with Ca2+-related PICs being a significant factor. By utilising computational motoneuron models, this thesis will explore the influence of PICs in explaining the observed changes in motor neuron activity among SCI patients following cathodal tsDCS. The goal is to establish a quantifiable metric that characterises the impact of specific stimulation therapies, providing a valuable tool for clinical applications. Specifically, this project focuses on identifying the firing characteristics associated with tsDCS in experimental data and analysing the sensitivity of the model parameters in explaining these features.

KEYWORDS

Spinal cord injury, transcutaneous electrical stimulation, persistent inward current, spasticity

1 INTRODUCTION

1.1 Physiology of motor control

The spinal cord is part of the central nervous system (CNS). It is responsible for the communication between alpha-motoneurons (MNs) and the cortical structures (such as the brain and cerebellum. The alpha-motoneurons are the final common pathway through which the CNS translates commands into specific motor actions. Understanding the dynamics of motoneurons is crucial in comprehending the smooth coordination and execution of movements.

When the central nervous system (CNS) wants to initiate muscle contraction, it sends electrical signals in the form of action potentials down to the axon of the motoneuron. At the end of the axon, neurotransmitters are released in the neuromuscular junction. The muscle will contract when neurotransmitters bind to receptors on the muscle fibres. The connection between the motoneuron and the muscle fibres allows the CNS to control muscle force and movement. [11]

The CNS regulates muscle force by adjusting the number and frequency of action potentials sent to the motoneurons. When more action potentials are sent, more neurotransmitters are released, leading to stronger muscle contraction. The frequency at which the action potentials are sent also affects the muscle contraction rate. When the action potentials are sent at a higher frequency, the muscle fibres do not have enough time to relax. This results in the summation of the signal, leading to a sustained and more forceful contraction. [11] According to Henneman's size principle, motor units are recruited based on the motor unit's size. Smaller motoneurons have a lower activation threshold and are recruited first. As greater force is required, larger motor units are sequentially recruited. [14]

1.2 Spinal cord injury and spasticity

Spinal cord injuries (SCI) disrupt this system, resulting in the loss of sensory-motor function below the injury site. SCI can result from direct injury to the spinal cord or damage to the surrounding tissues, with the severity and location of the injury affecting the degree of damage. After an SCI, patients often experience a range of symptoms arising from a loss of sensory-motor function below the injury side. Besides, the nervous system undergoes neuro-muscular adaptations, and spasticity emerges as a prevalent issue. [19]

A study showed that 65% of the patients experienced spasticity within the first 125 days after the injury. In the follow-up, after one year, this percentage decreased to 59% by treating the injury with either medication or chemodenervation of the spastic muscle(s). [16]. Spasticity is characterized by involuntary muscle contractions, increased muscle tone muscle stiffness and velocity-dependent reflex responses [1]. These are attributed to the increased excitability of the alpha-motoneurons located in the ventral horn. These neurons transmit signals from the brain to the muscles. [1]

The key mechanism underlying MN excitability is the presence of persistent inward currents (PICs). PICs in motoneurons are prolonged depolarising inward currents that can sustain action potentials even in the absence of a depolarising current and are primarily located in dendritic regions. They can amplify synaptic input up to five times [5]. Thus, PICs have a ability to change the motoneuron output to a given input drastically. [5, 12] In motoneurons, PICs are attributed to two ionic channels in the dendritic region: persistent sodium (Na^+) and L-type calcium (Ca^{2+}).The CaPIC activates slowly but is highly persistent, while the NaPIC is fast activating but tends to show more rapid inactivation. [12] Individuals with spasticity may exhibit alteration in PICs which often leads to overexpression or dysregulation of PICs. [5] Understanding the relationship between spasticity and PICs could provide insights into the mechanisms underlying this condition.

PIC influence the human motoneuron firing pattern in various ways. [12] :

(1) Self-sustained firing. This refers to the phenomenon where motoneurons generate action potentials without constant external signals. To determine if self-sustained firing is present, one can assess the point at which a motoneuron ceases to fire.
(2) Increase in excitability. The firing frequency increases when the motoneurons become more easily excitable due to PIC. PIC reduces the membrane potential closer to the threshold potential, making it easier for the motoneuron to initiate an action potential. The frequency at a constant input represents the steady state in motoneuron firing, where the influence of PIC on the firing rate and, thus, excitability becomes evident.
(3) Onset-offset hysteresis. The rate at which motoneurons transition between firing and non-firing can be used to assess the onset-offset mechanism. In the onset-offset hysteresis in PICs, their activation and deactivation happen at different voltage thresholds. This can cause the membrane potential to exceed a higher threshold to activate the PICs but only a lower threshold to deactivate them.

(4) Amplification and saturation. This feature is the phenomenon in which motoneurons gradually become more responsive to incoming signals until they reach saturation. The recruitment firing rate can show PIC's amplification and saturation mechanism.

PIC plays a significant role in the development of spasticity after spinal cord injury. In the acute stage of SCI, the disruption of signals from the brain to the spinal cord causes a reduction in the excitation of motoneurons. In the chronic stage of the injury, the excitability of the motoneurons increases, potentially due to PIC-related adaptations. In consequence, the temporary changes in the membrane potential of a neuron that make it more likely to generate an action potential can easily retrigger the PICs, resulting in strong, long-lasting reflexes and muscle stiffness. [5]

Several treatment options are developed to manage spasticity in individuals [1]. These include physical rehabilitation therapy [2], medication to reduce the intensity and frequency of spasms [17], surgical disruption of posterior roots to decrease peripheral reflex [7], and electrical stimulation techniques [15]. Transcutaneous spinal direct current stimulation has demonstrated a reduction of the index of spasticity [15]. It currently needs to be determined the effectiveness of stimulation treatments due to the lack of standardised stimulation parameters. To address this issue, a model-based approach is necessary to estimate the impact of motoneurons' excitability. Computer simulations have suggested applying direct and alternating electrical fields to the spinal cord to reduce motoneuronal hyperexcitability by modulating the dendritic PIC. [4, 5]

1.3 Transcutaneous spinal direct current stimulation

Transcutaneous spinal direct current stimulation (tsDCS) is a non-invasive technique that induces long-lasting neuromodulation in the human CNS. Electrodes are placed on the skin of the human torso at the back of the spine and somewhere else on the torse. A low-intensity direct electrical current flows through the spinal cord using this method. The physiological mechanisms underlying the effects of tsDCS have yet to be completely understood, so its clinical application remains limited. [3, 8] tsDCS aims to restore motoneurons' hyperexcitability by targeting Ca2+ channels [9, 22].

A study on rats explored how tsDCS affects motor neurons. Cathodal tsDCS (c-tsDCS) increased motor firing and caused a lasting effect after stimulation. Anodal tsDCS (a-tsDCS) also increased motor firing but had a temporary impact. Blocking calcium channels reduced c-tsDCS's lasting influence. A two-compartment neuronal model replicated the observed differences and supported the experimental findings, suggesting c-tsDCS enhances motor neurons by targeting calcium channels. [22] Based on the variety of stimulation protocols available, a model-based strategy to attain optimal motor recovery is the most effective.

1.4 Neuronal modelling

Single-compartment conductance-based models have shown that sodium and calcium persistent inward currents cause plateau potentials resulting in prolonged self-sustained firing in mice after SCI [10]. Recent research on two-compartment models indicates a greater and longer-lasting response during and after cathodal-tsDCS compared to anodal-tsDCS. Additionally, the use of reduced Ca^{2+} decreased response during cathodal-tsDCS and elimination of the persistent response. [22]

Computational models pushed forward the state of the art regarding the search for a model-based strategy to attain optimal motor recovery. It is currently difficult to develop models that account for the variability in human neural systems, as individuals can exhibit significant differences. Factors like age, injury type, and genetic predisposition can contribute to this variation, limiting the effectiveness of specific models.

Moving beyond generic mice-derived models [10], subject-specific modelling of motor neurons is a promising approach to improve the accuracy of predictions of the influence of tsDCS on spasticity. Customised models are designed for individual patients, considering the natural variations in human physiology. This approach provides a more accurate representation of neural behaviour. It is essential to recognise that even though they have potential, current subject-specific models of MNs [20, 21] remain limited in scope. Predominantly focused on a single-compartment structure and passive properties, these models simplify the intricate dynamics of MNs, underscoring the need for further advancements to capture the full complexity of neuronal behaviour.

This research aims to bridge a gap by combining experimental data with two-compartment models where PICs are included to study the effects of tsDCS on PICs in spinal cord injury subjects. Firing features related to PIC (recruitment and derecruitment threshold and discharge rate, and plateau discharge rate) will be identified in the experimental data, and the sensitivity of the motoneuron model parameters will be tested to capture these features. This could have significant implications for understanding motor dysfunction mechanisms after spinal cord injury and developing targeted interventions to modulate neuronal excitability and improve motor recovery.

2 METHODS

2.1 Experimental protocol

Two patients with chronic incomplete SCI were positioned on a medical chair throughout the experiment. They were securely fastened to the chair, and the upper leg was immobilised at a 90° hip angle by attaching it firmly to a sturdy frame. An isometric ankle joint plantar-flexion force was measured using a force platform (Advanced Mechanical Technology, Inc., Watertown, USA) positioned near the chair to ensure the ankle was stably placed at 90° ankle and knee angles.

To determine maximum voluntary contractions (MVCs), patients generated as much plantarflexion force as possible by activating the gastrocnemius and soleus muscles for at least 5 seconds. This process was repeated thrice with a 1 to 2-minute rest between trials. The highest force achieved among the three trials was considered the MVC.

Patients underwent two types of stimulation: cathodal (2.5 mA) and sham transcranial direct current stimulation (tsDCS), in a randomised sequence. The electrode setup was identical for both cathodal and sham stimulation. The cathode electrode was positioned between the 11th and 12th thoracic vertebrae, and the anode electrode

was placed on the right shoulder. A custom-built direct-current stimulator (TMS International B.V., Oldenzaal, The Netherlands) controlled the stimulation while patients engaged in a force-tracking task for 15 minutes. This task involved 8 minutes of reference force tracking with 3.5 minutes of rest before and after the tracking exercise.

The impact of tsDCS was examined at three different times: before (pre), immediately after (t0), and 30 minutes after (t30) stimulation. Patients completed ramp-and-hold tasks during each phase, including nine sub-maximal plantar flexion contractions at 8%, 15%, and 20% of MVC (three tasks per level, in random order) as in figure 1. A single task consisted of a ramp-up phase (2.5% MVC/s), a holding phase (25 seconds), and a ramp-down phase (2.5% MVC/s).

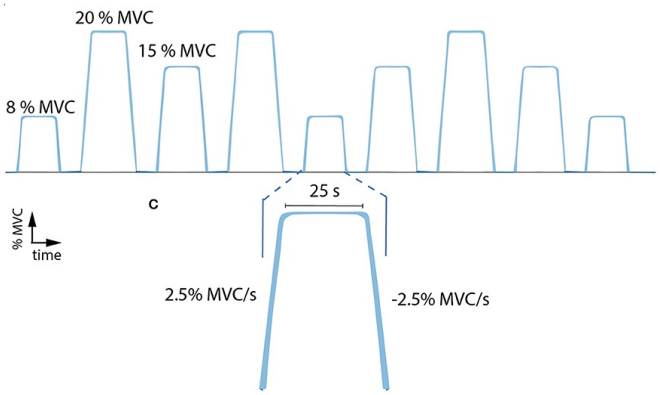

Figure 1: An example of tracking force tasks in different time conditions (pre, t0, t30). [9]

Throughout each phase, high-density electromyograms (HD-EMGs) were recorded using a TMSi Refa multi-channel amplifier (TMS International B.V., Oldenzaal, The Netherlands) at a sampling rate of 2048 Hz. Two sets of 8x8 electrode grids with inter-electrode distances of 8 mm and 3 mm were placed on the gastrocnemius medialis and soleus muscles, respectively. These grids were attached to the skin using 1-mm thick bi-adhesive foam layered with conductive paste to improve skin-grid contact. The reference electrode was positioned on the fibula.

2.2 Data processing

High-density electromyograms of the soleus were filtered using a 20 to 500 Hz zero-phase Butterworth filter. These signals were then separated into individual spike trains using convolution kernel compensation blind source separation [23]. Each resulting spike train was represented as a binary vector where ones denoted a spike event, while zeros indicated no firing activity.

The decomposed spike trains underwent a quality-control using a quality control algorithm [9]. This algorithm enforced specific criteria: the pulse-to-noise ratio needed to be greater than 20 dB, the coefficient of variation had to be less than 0.3, and discharge rates should not exceed 30 Hz. These thresholds were chosen to eliminate spike trains that did not originate from physiological processes while retaining a meaningful amount of data per trial. Motor neurons that did not meet these criteria were excluded from further analysis.

2.3 Motoneuron modelling

The motoneurons are described as a two-compartment motoneuron model including an L-type Ca^{2+} channel. The corresponding electrical circuit of the model is shown in figure 2 and consists of a somatic and dendritic compartment. The cell membrane capacitance and resistance properties are modelled to represent the neuron's electrical behaviour. In this model $g_{L,x}$ is the leakage conductance, E_L the leakage Nernst potential, g_{Na}, g_{Kf} and g_{Ks} the maximal ionic conductances. [6]

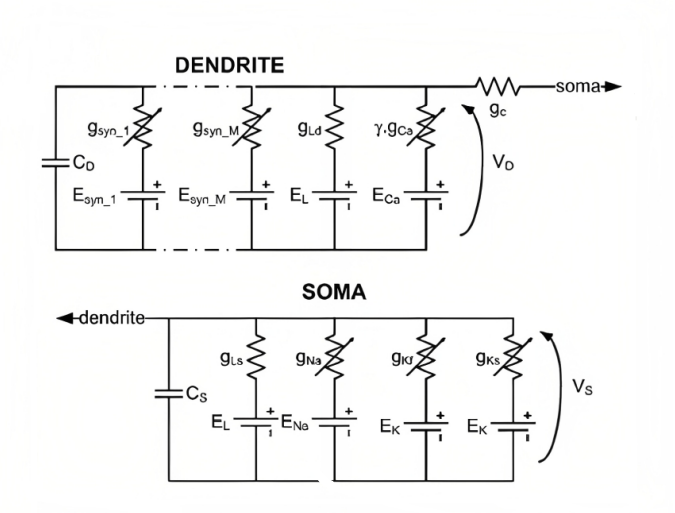

Figure 2: Electrical circuit of a two-compartment MN model representing soma and dendrite. [6]

The model follows the Hodgkin-Huxleyu formation and uses a pulsed-based method to solve them. This pulse-based method characterises the dynamics of the calcium current based on alphaP and betaP. *betaP* is the backward rate constant that plays a role in determining the kinetics of the state variables, which are components of mathematical descriptions used to model the behaviour of ion channels according to Hodgkin-Huxley type models. betaP is the backward rate constant for the activation variable corresponding to PICs and influences how quickly the activation variable returns to its resting state after being activated.*gCa* is the maximal ionic conductance of calcium (in $\mu S/cm^2$). Calcium plays a crucial role in neuronal excitability. gCa can potentially impact the strength of calcium-dependent currents, including PICs. *gCoupling* is the coupling conductance between the somatic and dendritic compartments (in μS). The conductance between the soma and dendrites impacts connectivity and communication levels. This can influence the propagation of signals, including PICs, between these dendrites and soma. γ represents the level of neuromodulation from the descending monoaminergic pathways. When $\gamma = 0$, there is no PIC present. By investigating these active parameters in the computational model (*betaP*, *gCa*, *gCoupling*, γ), we can investigate how

changing these parameters could affect the firing patterns of the motoneurons. [6]

2.4 Analysis

Different tests are performed to analyse the experimental data and the model parameters.

Test 1: Soma size-dependent influence of model parameters. The passive properties of the motoneuron pool were determined using metaheuristic optimisation of biophysically realistic motoneuron models [21]. The smallest and largest motoneuron are selected. These motoneurons are simulated with the parameters *betaP*, *gCa* and *gCoupling* linearly fitted to the soma-sizes while gradually increasing *gamma* with steps of 0.25 until self-sustained firing is observed, which is when the motoneuron continuously fires after the offset of force. The time of offset of force is determined by first filtering the force profile with a *movmean* filter with window size 1000. Next, the approximate derivative is determined using the *diff* function. The offset of force occurs when the approximate derivative is below the threshold of -0.0005.

Test 2: Identification of PIC-related firing features in the experimental data. Spike trains were analysed by calculating the features: threshold of recruitment and derecruitment, discharge rate at recruitment, derecruitment and plateau. The threshold of recruitment and derecruitment is defined as the % MVC where the motoneuron respectively starts and stops firing. =When determining the discharge rate during recruitment, we count the spikes within the initial second of motoneuron firing. Similarly, when calculating the discharge rate during derecruitment, we count the spikes within the final second of motoneuron firing. The discharge rate during the plateau is calculated by dividing the spikes by the plateau's period. The plateau is the period where the force profile is constant and not equal to zero. The force profile is therefore filtered with a *movmean* filter with window size 1000, and the force is considered constant when the filtered signal is beneath a threshold of 0.0004. For each repetition of the experiment, the average and standard deviation of the active motoneurons' features during the repetition are computed for both subjects.

Test 3: Sensitivity of the motoneuron model parameters. To assess the individual impact of the parameters betaP, gCa, gCoupling, and gamma, the parameters betaP, gCa, gCoupling, and gamma are modified in the ranges specified in table 1 using a Latin Hypercube Sampling (LHS) method [13]. This approach allows for extracting a large amount of sensitivity information with a relatively small sample size. With these parameters, the model will simulate the motoneuron behaviour for the largest and smallest motoneuron where the passive properties are determined using the metaheuristic optimisation of the motoneuron models [21]. The features of the motoneuron (threshold of recruitment and derecruitment, discharge rate at recruitment, derecruitment and plateau) are calculated in the same way described in test 2. The linear correlation between the parameters and the model's features is calculated using the Pearson Correlation Coefficient, and the non-linear correlation is calculated using the Spearman Correlation Coefficient [13].

Table 1: Ranges of the model parameters for testing the sensitivity of the motoneuron model

Parameter	Range
gCa	[0.04, 0.02]
gCoupling	[0.01, 0.3]
betaP	[0, 0.1]
gamma	[0, 4]

Test 4: Firing characteristics modulation A grid sampling method is used to simulate the motoneurons behaviour for the largest and the smallest motoneuron. The grid sampling method is a way to explore the multi-dimensional parameter space of the model systematically. This approach involves discretising the parameter space into a grid by defining ranges and step sizes for each parameter. The gCa, gCoupling and betaP ranges are shown in table 1. Notably, the gamma parameter spans from 0 to 2.5 and 0 to 4 for smaller and larger motoneurons, respectively. This grid-based sampling strategy will use five discrete points for each parameter. The firing features (recruitment and derecruitment threshold, discharge rate at recruitment, derecruitment and plateau) are calculated for each possible combination of parameters to find the modulation of the features caused by the change in parameters.

3 RESULTS

3.1 Soma size-dependent influence of model parameters

The passive properties of the motoneuron pool of subject 1 are shown in figure 3 and include betaQ, alphaQ and soma diameter (Ds). From this optimisation, the smallest and the largest motoneuron are selected. The passive properties of these motoneurons are shown in table 2.

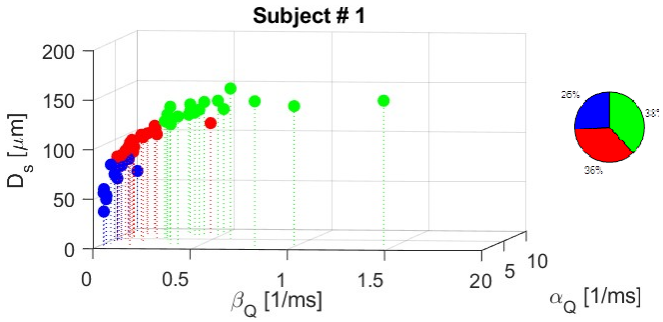

Figure 3: Subject-specific in vivo motoneuron properties identified by the optimisation framework with three clusters of parameters. [21]

Table 2: Passive properties of the smallest and largest motoneuron within the motoneuron pool

	betaQ [1/ms]	alphaQ [1/ms]	Diameter Soma [μm]
Smallest MN	0.0131	1.8911	33.7682
Largest MN	13.8620	2.3552	158.982

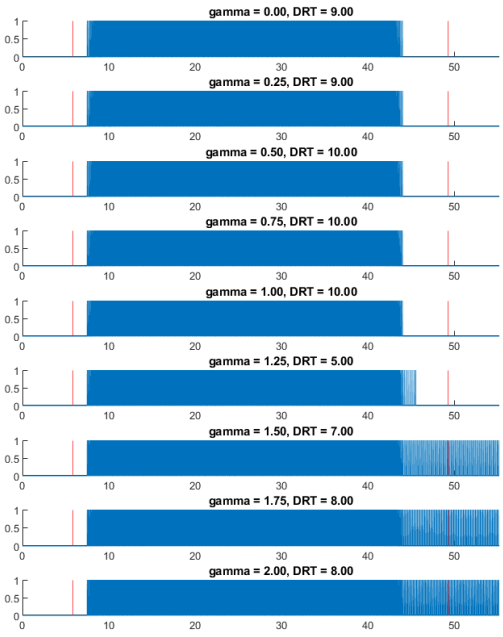

Figure 4: Motoneuron spike trains for MN with a soma-size of 33.77μ**m and gamma values between** 0.00 **and** 2.00

The figures 4 and 5 depict the motoneuron spike trains as the gamma increases for the smallest and largest motoneuron, respectively. The smallest motoneuron in the motoneuron pool achieves self-sustained firing at a gamma of 1.50. The discharge rate at derecruitment seems to reach a constant value of 8.00 Hz. The largest motoneuron achieves self-sustained firing at a gamma of 4.00. The discharge rate at recruitment is increasing but seems to reach a constant value for higher gammas.

3.2 Identification of PIC-related firing features in the experimental data

The experimental data shows differences between the sham and cath conditions regarding the baseline of excitability. To assess the influence of the stimulation on the selected features, the prestimulation, t0 and t30, are plotted in figure 6. In this figure, the columns correspond to different subjects, while each row reflects a specific feature. The colours represent the different force profiles the subject performed, and each figure shows the cathodal influence on the left side and the sham influence on the right side. The slope represents the stimulation's effect on the selected features.

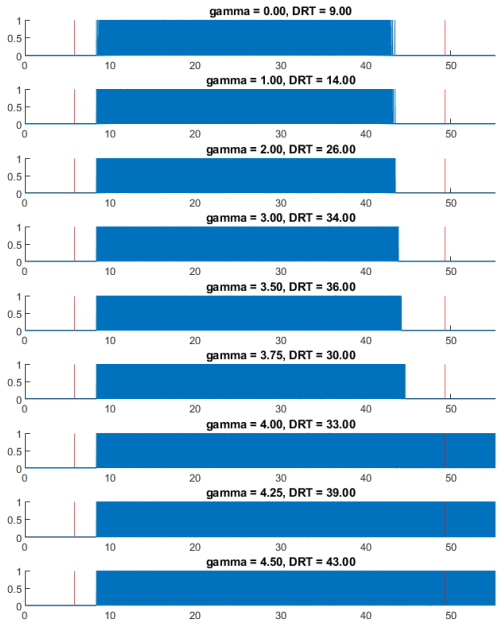

Figure 5: Motoneuron spike trains for MN with a soma-size of 158.98μ**m and gamma values between** 0.00 **and** 4.50

The behaviour of the motoneuron pool depends on the average number of decomposed active motoneurons during a specific condition across three trials. Refer to appendix .1 for a comprehensive breakdown of the total number of motoneurons for each trial of each condition. Additionally, table 4 provides an overview of the average number of motoneurons. It can be seen that subject two has significantly less decomposed active motoneurons compared to subject 1. Moreover, the sham conditions have slightly more decomposed active motoneurons than the cathodal condition for both subjects.

Table 3: Average number of decomposed motoneurons over all trials for each condition.

		Subject 1		***Subject 2***	
Time	**% MVC**	*Cath*	*Sham*	*Cath*	*Sham*
Pre	8	6.33	9.33	2.33	3.33
	15	7.33	10.33	2.66	5
	20	7.33	9.33	3	5.66
t0	8	7	8	3	5.66
	15	7	9	3	5
	20	8.33	8.33	3	6
t30	8	7.66	9.33	3.66	7
	15	9	9.66	3.33	3.66
	20	7.66	9.33	3.33	5
Avg		7.48	9.19	3.04	5.11

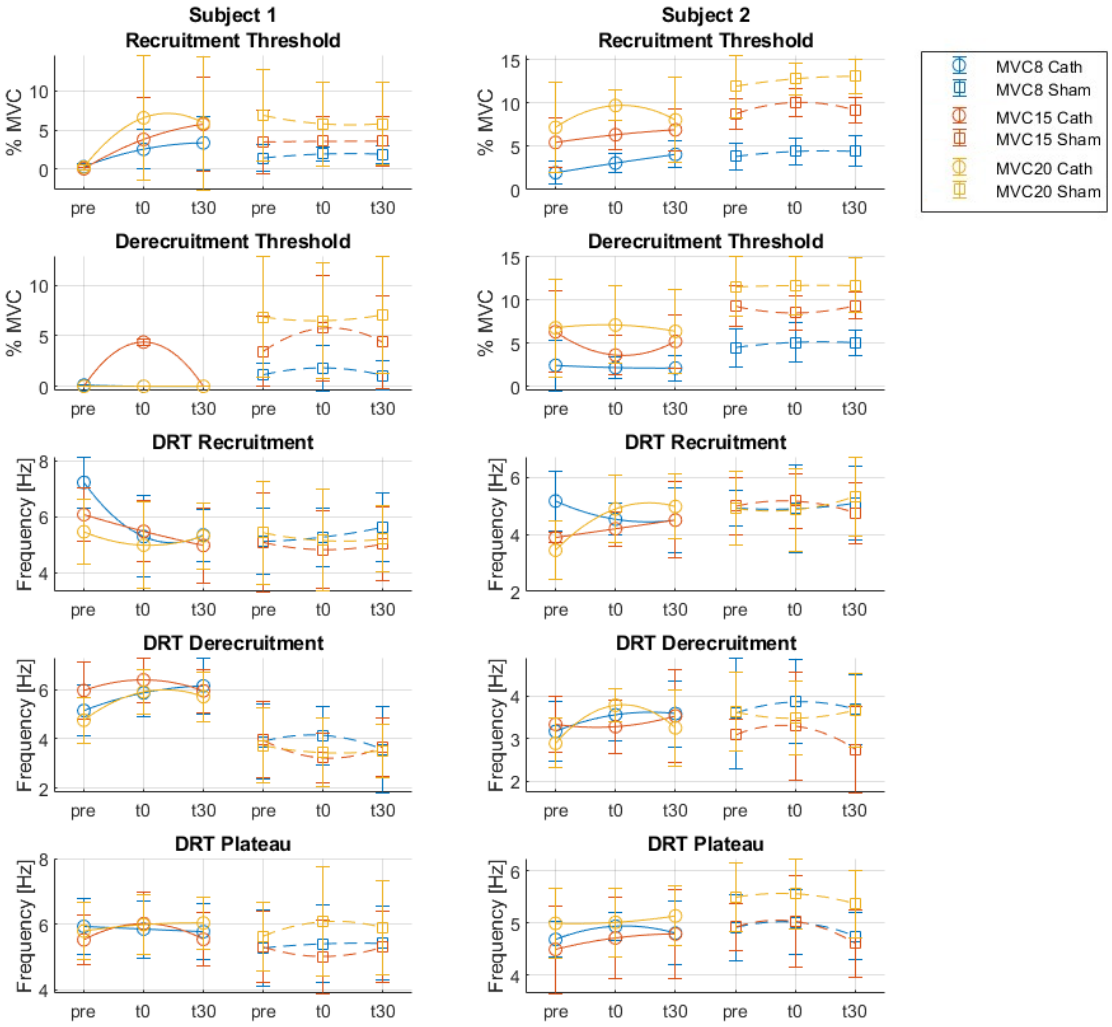

Figure 6: Comparing the cath (left) and sham (right) conditions on the selected features for 8%, 15% and 20% MVC for both subjects before the stimulation (pre), right after the stimulation (t0) and 30 minutes after the stimulation (t30)

The cathodal slopes in figure 6 show an increased recruitment threshold immediately after stimulation. The stimulation's effect decreases after 30 minutes. The sham slopes stay relatively constant. The derecruitment threshold slightly decreases by cathodal stimulation for subject 1, except for a 15% MVC. For subject 2, the derecruitment threshold also decreases for the cathodal condition and stays relatively constant or increases for the sham stimulation.

The discharge rate at recruitment is clearly decreasing for subject one during the cath condition but shows an upward trend for subject 2. For the sham conditions, the discharge rate at recruitment seems to drop slightly for subject 1 but stays constant for subject 2.

The discharge rate at derecruitment increases during the cathodal condition and decreases for the sham condition. This can be most clearly seen in subject 1. The discharge rate at the plateau slightly increases for both subjects during the cathodal condition and somewhat decreases for the sham condition.

3.3 Sensitivity of the motoneuron model parameters

Figures 7 and 8 show the linear and non-linear correlation coefficients between the input parameters and the output features. The colours of the heatmap indicate how strong the correlation is, with red as a strong positive correlation and blue as a strong negative correlation.

The parameter gCa does not show a linear or non-linear correlation with any of the output features of the model.

The recruitment threshold is sensitive to changes in gCoupling, where gCoupling has a more extensive influence on the larger motoneurons. No other parameters have an impact on the recruitment threshold.

The derecruitment threshold is mainly affected by betaP and gamma. Where betaP has a positive linear correlation and gamma has a negative linear correlation, both with a more substantial influence on the larger neurons. When looking at the non-linear correlation, we can see that betaP has a positive impact, and gamma has a negative effect on the larger motoneurons. There is no non-linear correlation for the derecruitment threshold of small motoneurons.

The discharge rate at recruitment and derecruitment have a positive (non-)linear correlation with gCoupling for large neurons but is negative for small neurons. betaP has a strong negative (non-linear) correlation with the discharge rate at recruitment and derecruitment. The discharge rates for larger neurons are strongly influenced by gamma. Here we can see a stronger non-linear correlation than a linear correlation.

The discharge rate at the plateau is strongly influenced by gCoupling, with a more substantial impact on the larger motoneuron. Here, we can see a stronger non-linear correlation than a linear correlation.

3.4 Modulation of firing features

Figures 9 and 10 display a selection of the figures found in appendix .2 to evaluate the significant effects of input parameters on the features for large and small motoneurons.

BetaP and gamma do not affect the recruitment threshold, but the gCoupling increase lowers it for both the largest and smallest motoneuron. The relationship between betaP and the derecruitment threshold remains consistent if gCoupling is zero for the largest neuron. However, as gCoupling increases, the threshold begins to decrease for lower values of betaP, with a more significant impact on lower gCa values. Furthermore, when gamma increases, the threshold reaches zero for lower betaP and gCa values. This applies to both the biggest and smallest motoneurons.

For the largest motoneuron, when looking at the discharge rate during recruitment and derecruitment in relation to the betaP parameter, a clear negative exponential relationship can be observed when gamma is not equal to zero. It is interesting to note that the strength of this relationship becomes more prominent as either gamma or gCoupling values increase. This suggests that alterations in the parameters gamma and gCoupling amplify the intensity of the negative exponential correlation between discharge rate at recruitment and betaP. The parameter gCa slightly changes the slope of the curves. The relationship still exists for the smallest motoneuron, although it is not as strong.

By analysing the discharge rate at the plateau for the largest motoneuron in relation to the betaP parameter, we can observe that the correlation shifts from a positive to a negative logarithmic relationship as the gCoupling increases. Moreover, when gamma increases, the relationship between betaP and the discharge rate at the plateau becomes slightly stronger. The parameter gCa slightly changes the slope of the curve. The relationship between the smallest motoneuron still exists, but only for larger values of gamma.

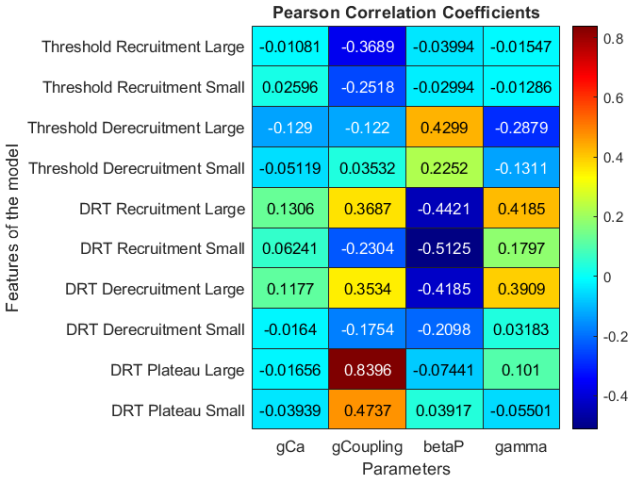

Figure 7: Pearson Correlation matrix showing the linear correlation coefficients between the input parameters (gCa, gCoupling, betaP, gamma) and the output features of the model using an LHS method.

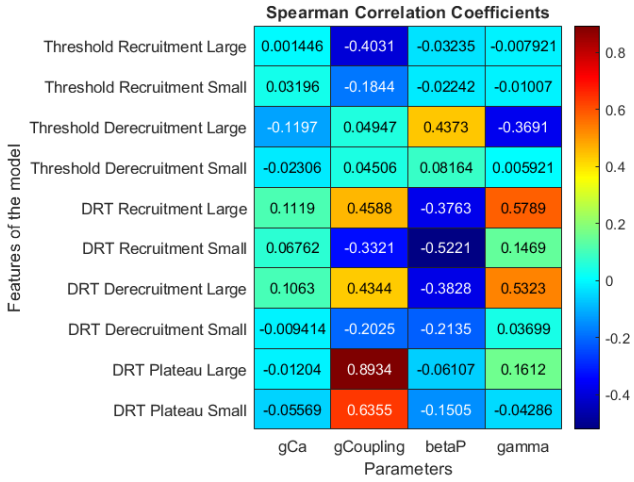

Figure 8: Spearman Correlation matrix showing the non-linear correlation coefficients between the input parameters (gCa, gCoupling, betaP, gamma) and the output features of the model using an LHS method.

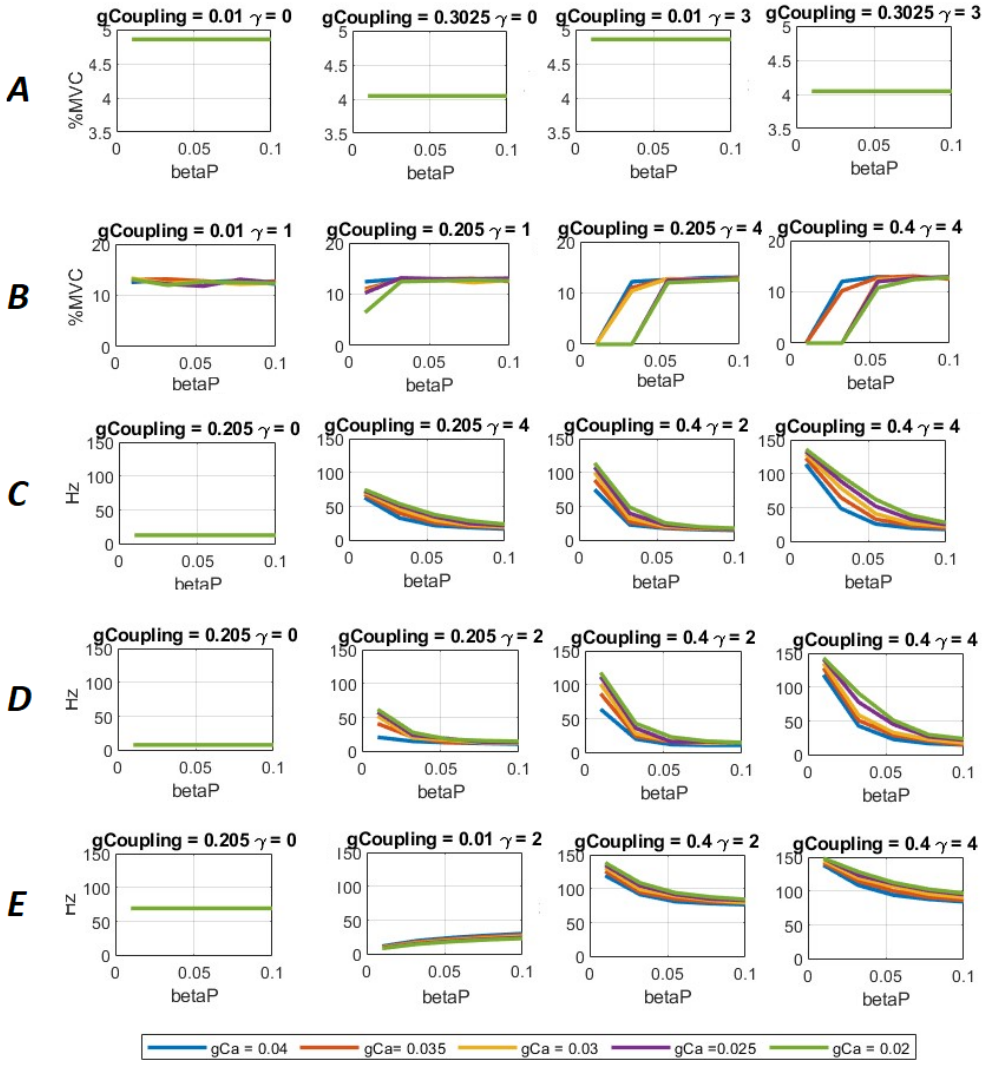

Figure 9: Relationship of the input parameters on (A) Recruitment threshold, (B) Derecruitment threshold, (C) DRT at recruitment, (D) DRT at derecruitment, (E) DRT at plateau, for the largest motoneuron

4 DISCUSSION

The research findings indicate that tsDCS can modify the firing of motoneurons via PICs, which offers a promising opportunity for regulating motoneuron excitability for spasticity.

This work shows a potential relationship between gamma's impact and the motoneurons' size. Modulation of PIC activity across the motoneuron pool was expected to have a different effect, as low-threshold motoneurons rely heavily on lasting PICs to maintain their firing [18].

Only the experimental data before, immediately after and 30 minutes after the stimulation is available, so we calculate the features at only three points in time. Therefore, statistical analysis to assess the influence of the stimulation may have limited or no statistical power. It is essential to account for the differences in excitability between the sham and cathodal conditions to ensure fair comparisons and accurate interpretations. One way to address this problem is through a normalisation method, which can standardise the observed variations in excitability by establishing a common baseline. This approach will isolate the specific effects of cathodal stimulation, making the results more reliable.

The observed changes in recruitment and derecruitment thresholds following cathodal stimulation offer interesting insights into the underlying mechanisms. The increase in the recruitment threshold might be explained by the warm-up time associated with persistent inward currents. During the initiation of cathodal stimulation, there may be a brief period where the motoneuron's responsiveness gradually adjusts to the changed polarisation state. This can lead to an increase in the recruitment threshold. [12] The decrease

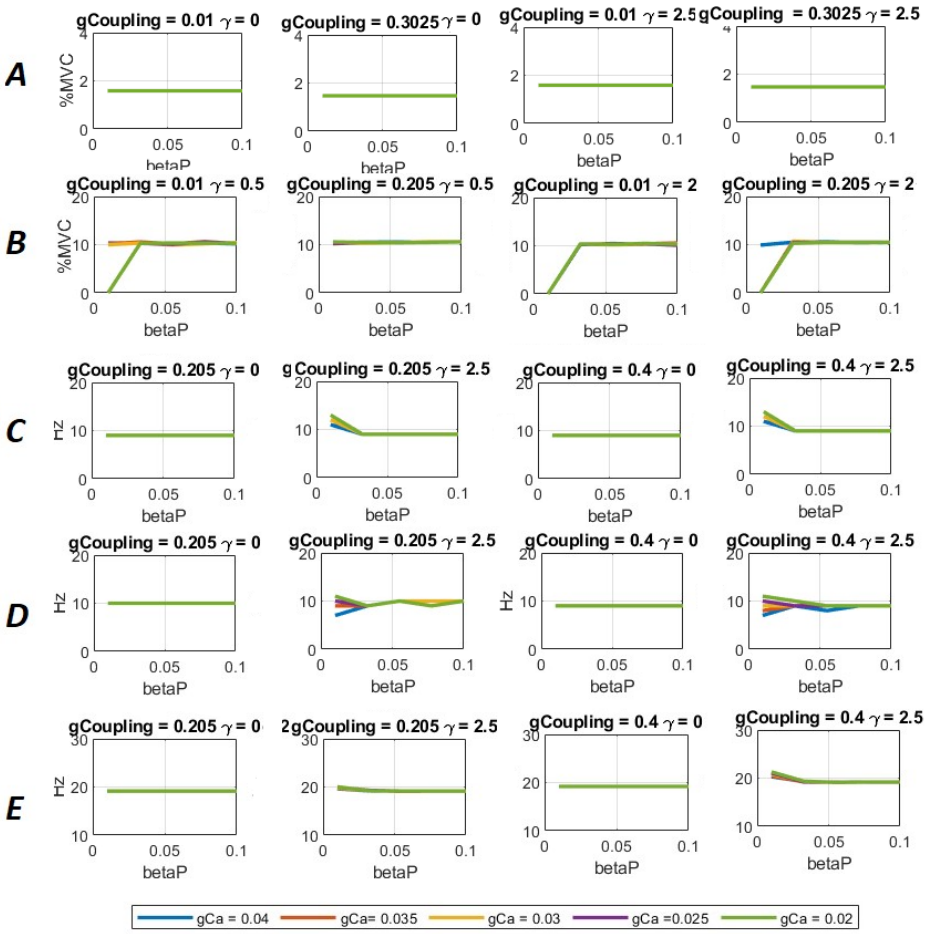

Figure 10: Relationship of the input parameters on (A) Recruitment threshold, (B) Derecruitment threshold, (C) DRT at recruitment, (D) DRT at derecruitment, (E) DRT at plateau, for the smallest motoneuron

in derecruitment threshold observed under cathodal conditions, as compared to sham, could be caused by the sustained firing activity induced by PIC [12]. Moreover, the observed frequency differences in recruitment and derecruitment between cathodal and sham conditions could be attributed to onset/offset hysteresis. The stimulation-induced changes might introduce delays in the initiation and termination of firing, contributing to differences in firing frequencies between the two conditions. [12]

Acknowledging that the experimental results are derived from a limited number of motoneurons is essential. The limited number of motoneurons may only partially represent part of the motoneuron pool. Additionally, the decomposition algorithm is biased to decompose the smaller motoneurons earlier [23]. This emphasises the need for caution when interpreting the results and underscores the potential value of exploring alternatives or improving the current decomposition method.

To assess the modulation of the firing features, a grid sampling method is used to explore the parameter space. It is essential to note that it might overlook finer nuances between grid points [13]. To address this limitation, future analyses need to focus on techniques that provide better accuracy in determining the most suitable parameter values.

We suggest a constrainment where gamma can only have two values: 0, which means no electrical stimulation, and 1, which indicates that stimulation is present. The three parameters - gCoupling, betaP, and gCa - would be fine-tuned through optimisation techniques to replicate the firing behaviour closely. By adjusting these parameters, we aim to create a model that can accurately imitate the complex firing patterns of motoneurons in SCI patients. This will offer valuable insights into the underlying dynamics and improve our understanding of the system's behaviour.

We propose to ensure that the minimum value of gCoupling is above 0.01. This is because no feature modulation is observed when gCoupling is 0.01. However, it is still being determined from which value the modulation will appear—considering that when

gCoupling values are less than 0.205, there's a positive logarithmic relationship between the discharge rate at the plateau and betaP. Still, this relationship becomes negative for values above 0.205. When setting the upper boundaries for gCoupling and betaP, it's essential to consider the modulation of the discharge rate. If gCoupling is set too high, the discharge rate can become unrealistically high. Besides, considering that the discharge rate may become too high when betaP values are low is important. To establish precise upper and lower boundaries, we need to use a more refined sampling technique that will enable us to attain higher resolution.

5 CONCLUSION

In conclusion, our proposed constrainment, which assigns gamma the discrete values of 0 and 1 to represent the absence and presence of electrical stimulation, offers a novel approach to understanding and mimicking the firing behaviour of motoneurons. By carefully fine-tuning the parameters gCoupling, betaP, and gCa using optimisation techniques, we can aim to create a computational model replicating the intricate firing patterns observed in experimental data of the motoneurons of spinal cord injury (SCI) patients.

Our results explain the influence of the parameters gCa, betaP, gCoupling, and gamma on critical aspects of firing behaviour, including the threshold of recruitment and derecruitment, as well as the discharge rate at recruitment, derecruitment, and plateau phases. By systematically exploring the impact of these parameters on the features associated with PIC in our computational model, we gain valuable insights into how tsDCS modulates these features in motoneurons.

By gaining an understanding of how different parameters interact and influence the characteristics associated with PIC, we have a better understanding of the impact of tsDCS on motoneuron behaviour. Such insights are crucial for advancing our knowledge of neuromodulation techniques and developing more targeted and effective treatments for managing spasticity in individuals suffering from spinal cord injuries. Ultimately, our research bridges the gap between experimental and computational application, clarifying the relationship between parameter manipulation and its impact on motoneuronal firing behaviour.

REFERENCES

[1] M M Adams and A L Hicks. 2005. Spasticity after spinal cord injury. *Spinal Cord* 43 (2005), 577–586. https://doi.org/10.1038/sj.sc.3101757

[2] T Albert and A Yelnik. 2003. [Physiotherapy for spasticity]. *Neuro-Chirurgie* 49, 2-3 Pt 2 (5 2003), 239–46.

[3] Filippo Cogiamanian, Maurizio Vergari, Francesca Pulecchi, Sara Marceglia, and Alberto Priori. 2008. Effect of spinal transcutaneous direct current stimulation on somatosensory evoked potentials in humans. *Clinical Neurophysiology* 119 (2008), 2636–2640. https://doi.org/10.1016/j.clinph.2008.07.249

[4] Sherif M. ElBasiouny and Vivian K. Mushahwar. 2007. Suppressing the excitability of spinal motoneurons by extracellularly applied electrical fields: insights from computer simulations. *Journal of Applied Physiology* 103, 5 (11 2007), 1824–1836. https://doi.org/10.1152/japplphysiol.00362.2007

[5] S M Elbasiouny, J E Schuster, and C J Heckman. 2010. Persistent inward currents in spinal motoneurons: Important for normal function but potentially harmful after spinal cord injury and in amyotrophic lateral sclerosis. *Clinical Neurophysiology* 121, 10 (10 2010), 1669–1679. https://doi.org/10.1016/j.clinph.2009.12.041

[6] Leonardo Abdala Elias, Vitor Martins Chaud, and André Fabio Kohn. 2012. Models of passive and active dendrite motoneuron pools and their differences in muscle force control. *Journal of Computational Neuroscience* 33, 3 (2012), 515–531. https://doi.org/10.1007/s10827-012-0398-4

[7] Johannes M. Nicolaas Enslin, Nelleke Gertrude Langerak, and Anthony Graham Fieggen. 2019. The Evolution of Selective Dorsal Rhizotomy for the Management of Spasticity. *Neurotherapeutics* 16, 1 (1 2019), 3–8. https://doi.org/10.1007/s13311-018-00690-4

[8] Felipe ID Fava de Lima, Cristiano Rocha Silva, and Andre Fabio Kohn. 2022. Transcutaneous spinal direct current stimulation (tsDCS) does not affect postural sway of young and healthy subjects during quiet upright standing. *PLoS ONE* 17, 4 (4 2022). https://doi.org/10.1371/journal.pone.0267718

[9] Antonio Gogeascoechea, Alexander Kuck, Edwin van Asseldonk, Francesco Negro, Jan R. Buitenweg, Utku S. Yavuz, and Massimo Sartori. 2020. Interfacing With Alpha Motor Neurons in Spinal Cord Injury Patients Receiving Trans-spinal Electrical Stimulation. *Frontiers in Neurology* 11 (6 2020). https://doi.org/10.3389/fneur.2020.00493

[10] Joe Graham, Victoria Booth, and Ranu Jung. 2005. Modeling motoneurons after spinal cord injury: persistent inward currents and plateau potentials. *Neurocomputing* 65-66 (6 2005), 719–726. https://doi.org/10.1016/j.neucom.2004.10.067

[11] C.J. Heckman and Roger M. Enoka. 2004. Physiology of the motor neuron and the motor unit. In *Handbook of Clinical Neurophysiology*. Vol. 4. Chapter 6, 119–147. https://doi.org/10.1016/S1567-4231(04)04006-7

[12] C. J. Heckman, Michael Johnson, Carol Mottram, and Jenna Schuster. 2008. Persistent inward currents in spinal motoneurons and their influence on human motoneuron firing patterns. , 264–275 pages. https://doi.org/10.1177/1073858408314986

[13] J.C. Helton, J.D. Johnson, C.J. Sallaberry, and C.B. Storlie. 2006. Survey of sampling-based methods for uncertainty and sensitivity analysis. *Reliability Engineering & System Safety* 91, 10-11 (10 2006), 1175–1209. https://doi.org/10.1016/j.ress.2005.11.017

[14] Elwood Henneman, George Somjen, and David O. Carpenter. 1965. Excitability and inhibility of motoneurons of different sizes. *Journal of Neurophysiology* 28, 3 (5 1965), 599–620. https://doi.org/10.1152/jn.1965.28.3.599

[15] Ursula S. Hofstoetter, William B. McKay, Keith E. Tansey, Winfried Mayr, Helmut Kern, and Karen Minassian. 2014. Modification of spasticity by transcutaneous spinal cord stimulation in individuals with incomplete spinal cord injury. *The Journal of Spinal Cord Medicine* 37, 2 (3 2014), 202–211. https://doi.org/10.1179/2045772313Y.0000000149

[16] Kaila A. Holtz, Rachel Lipson, Vanessa K. Noonan, Brian K. Kwon, and Patricia B. Mills. 2017. Prevalence and Effect of Problematic Spasticity After Traumatic Spinal Cord Injury. *Archives of Physical Medicine and Rehabilitation* 98, 6 (6 2017), 1132–1138. https://doi.org/10.1016/j.apmr.2016.09.124

[17] Mariko Kita and Donald E. Goodkin. 2000. Drugs used to treat spasticity. *Drugs* 59, 3 (2000), 487–495. https://doi.org/10.2165/00003495-200059030-00006

[18] Ricardo N. O. Mesquita, Janet L. Taylor, Gabriel S. Trajano, Jakob Škarabot, Aleš Holobar, Basílio A. M. Gonçalves, and Anthony J. Blazevich. 2022. Effects of reciprocal inhibition and whole-body relaxation on persistent inward currents estimated by two different methods. *The Journal of Physiology* 600, 11 (6 2022), 2765–2787. https://doi.org/10.1113/JP282765

[19] National Institute of Neurological Disorders and Stroke. [n. d.]. Spinal Cord Injury. https://www.ninds.nih.gov/health-information/disorders/spinal-cord-injury#

[20] R. Ornelas Kobayashi, A. Gogeascoechea, L. Joseph Tomy, E. Van Asseldonk, and M. Sartori. 2022. Neural data-driven model of spinal excitability changes induced by transcutaneous electrical stimulation in spinal cord injury subjects. In *IEEE International Conference on Rehabilitation Robotics*, Vol. 2022-July. IEEE Computer Society. https://doi.org/10.1109/ICORR55369.2022.9896517

[21] Rafael Ornelas-Kobayashi, Antonio Gogeascoechea, and Massimo Sartori. 2023. Person-Specific Biophysical Modeling of Alpha-Motoneuron Pools Driven by in vivo Decoded Neural Synaptic Input. *IEEE Transactions on Neural Systems and Rehabilitation Engineering* 31 (2023), 1532–1541. https://doi.org/10.1109/TNSRE.2023.3247873

[22] Weiguo Song and John H. Martin. 2022. Trans-Spinal Direct Current Stimulation Targets Ca2+ Channels to Induce Persistent Motor Unit Responses. *Frontiers in Neuroscience* 16 (4 2022). https://doi.org/10.3389/fnins.2022.856948

[23] Yue Wen, Simon Avrillon, Julio C Hernandez-Pavon, al , Chen Chen, Guohong Chai, WeiChao Guo, Francesco Negro, Silvia Muceli, Anna Margherita Castronovo, A Holobar, M A Minetto, and D Farina. 2014. Accurate identification of motor unit discharge patterns from high-density surface EMG and validation with a novel signal-based performance metric. *Journal of Neural Engineering* 11, 1 (1 2014), 016008. https://doi.org/10.1088/1741-2560/11/1/016008

APPENDIX

.1 Average number of motoneurons in each experimental trial

Table 4: Total number of MN during each trial for each condition

		Subject 1								***Subject 2***							
		Cathodal				*Sham*				*Cathodal*				*Sham*			
		Trial				Trial				Trial				Trial			
Time	**% MVC**	1	2	3	Avg	1	2	3	Avg	1	2	3	Avg	1	2	3	Avg
Pre	8	7	6	7	6.33	9	9	10	9.33	2	2	3	2.33	3	2	5	3.33
	15	7	7	8	7.33	9	12	10	10.33	3	2	3	2.66	6	4	5	5
	20	5	9	8	7.33	10	9	9	9.33	3	3	3	3	6	6	5	5.66
t0	8	7	7	-	7	11	6	7	8	3	4	2	3	5	7	5	5.66
	15	9	4	8	7	9	9	9	9	2	3	4	3	6	4	5	5
	20	8	8	9	8.33	9	6	10	8.33	3	3	3	3	7	5	6	6
t30	8	7	10	6	7.66	10	8	10	9.33	3	4	4	3.66	6	9	6	7
	15	8	11	6	9	11	9	9	9.66	4	3	3	3.33	4	2	4	3.66
	20	6	7	10	7.66	11	9	8	9.33	3	4	3	3.33	5	5	5	5
Avg					7.48				9.19				3.04				5.11

.2 Firing characteristics modulation

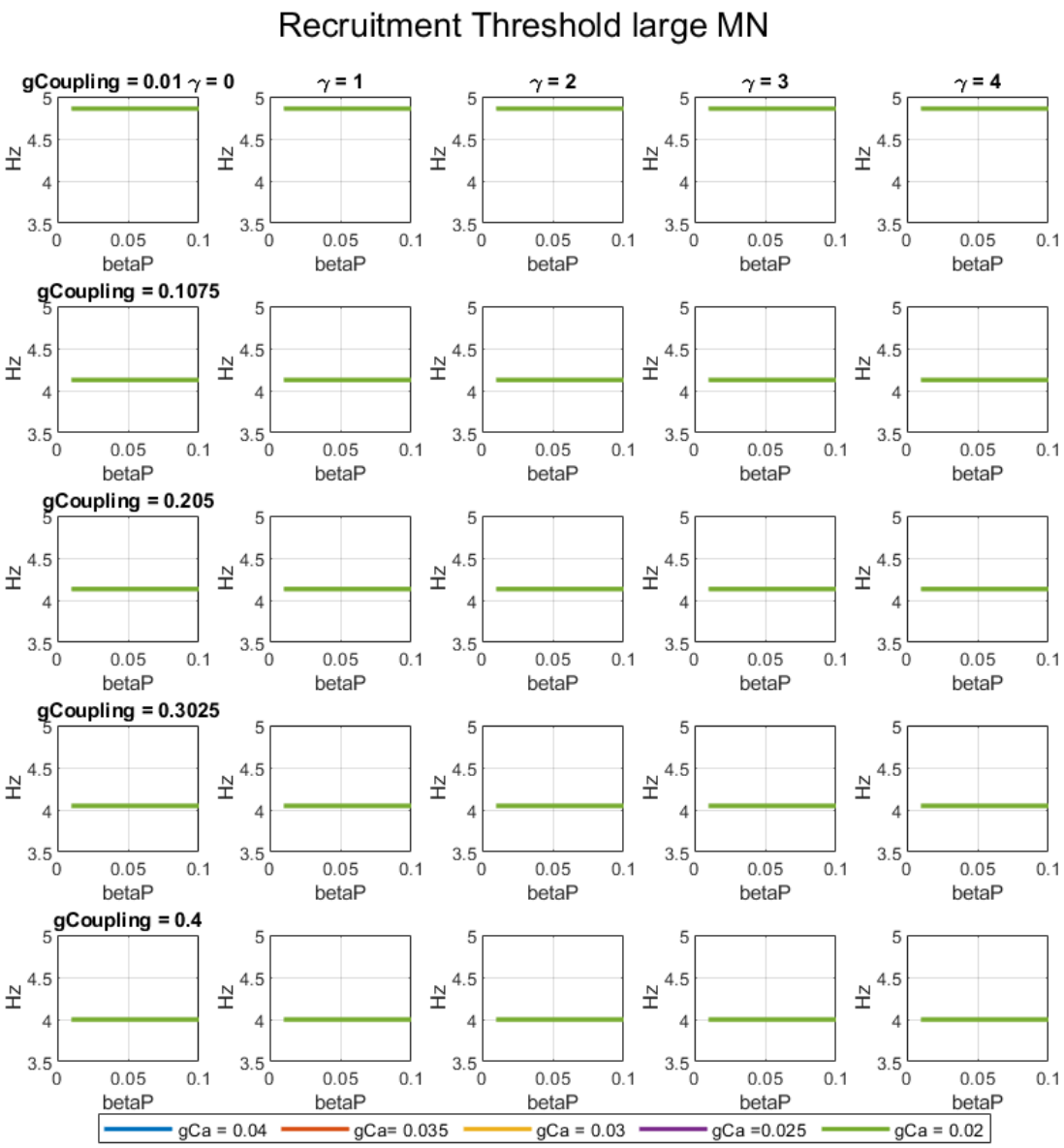

Figure 11: Modulation of the recruitment threshold for large motoneurons when changing gCa, gCoupling, betaP and gamma

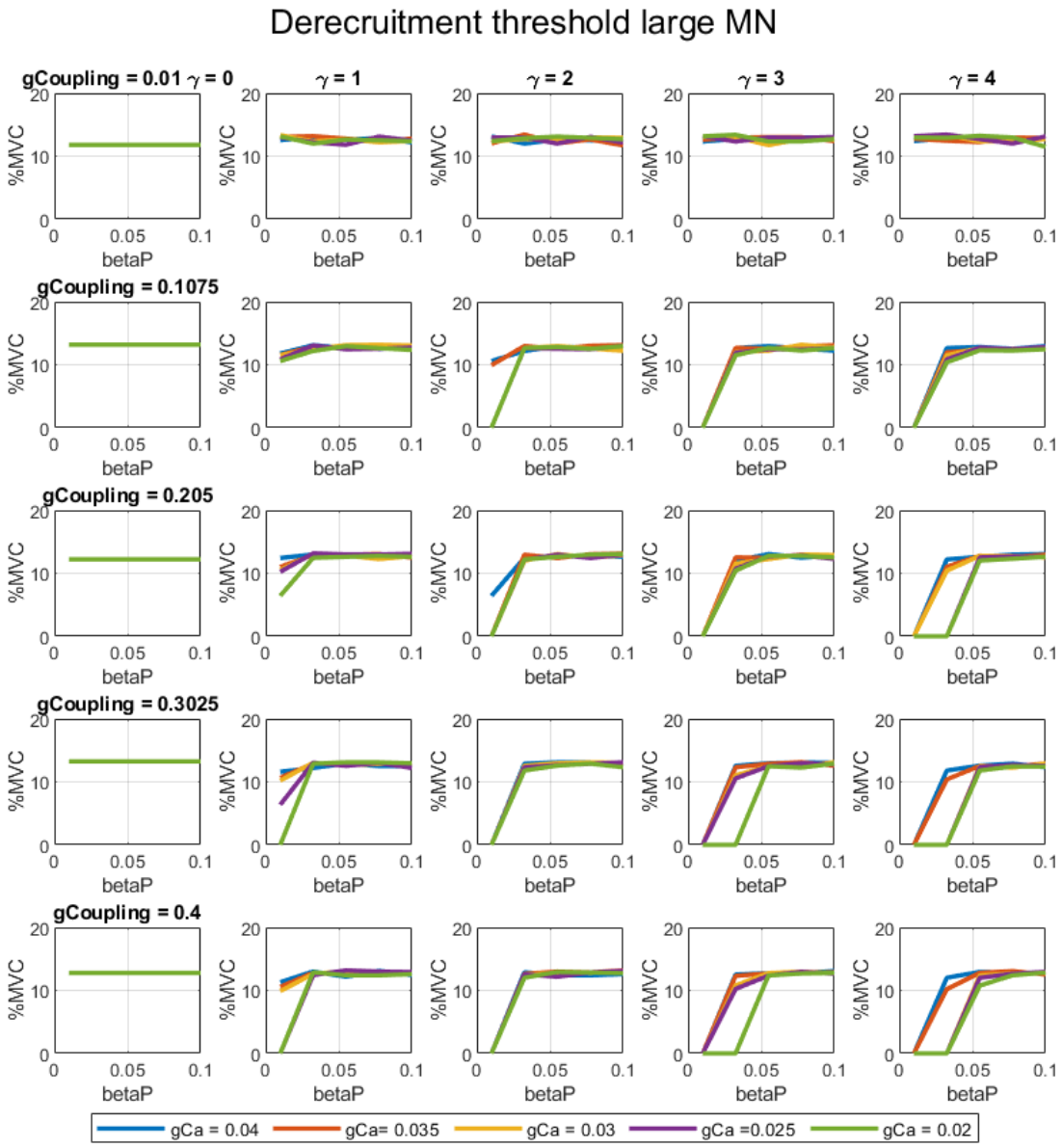

Figure 12: Modulation of the derecruitment threshold for large motoneurons when changing gCa, gCoupling, betaP and gamma

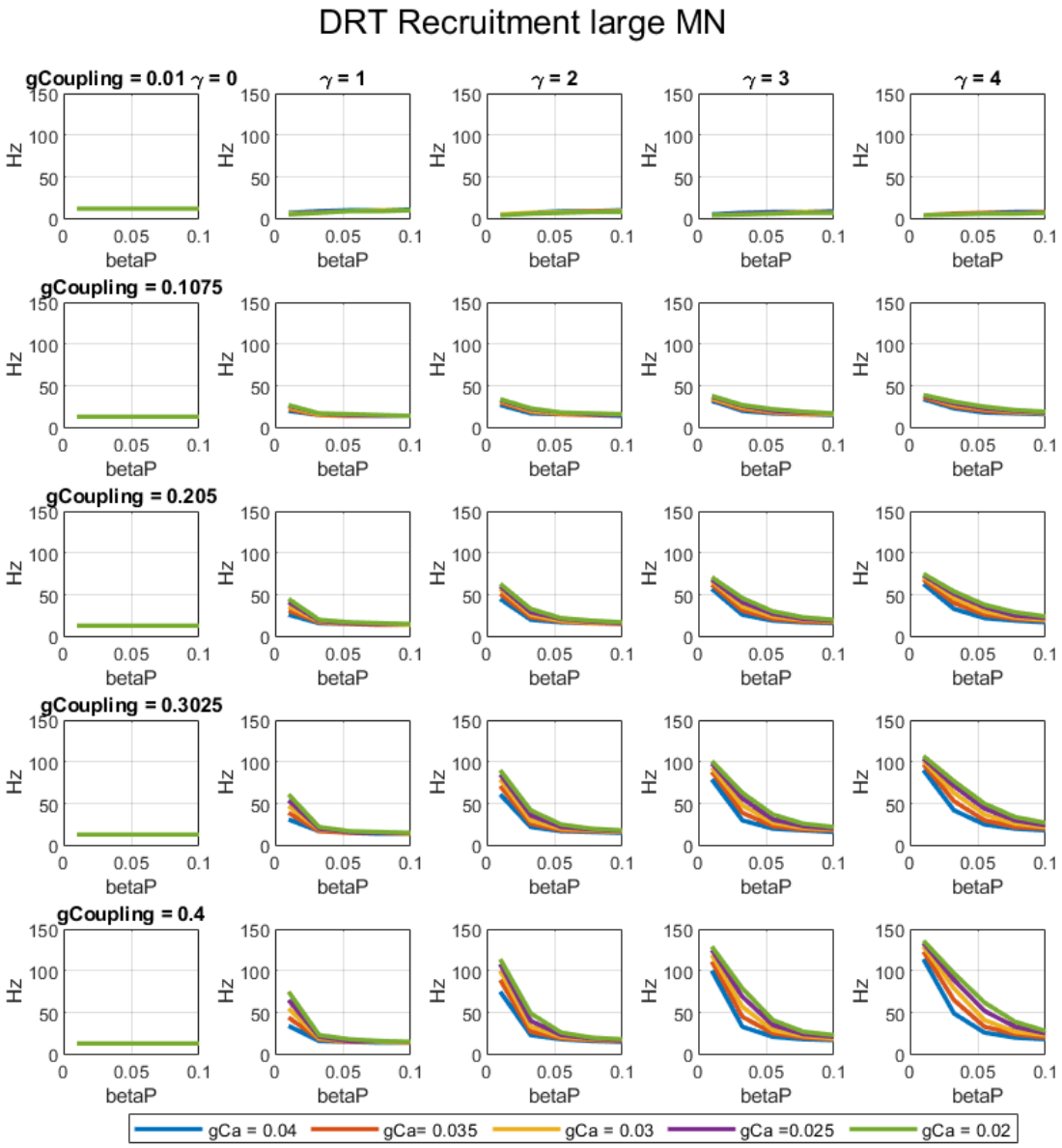

Figure 13: Modulation of the discharge rate at recruitment for large motoneurons when changing gCa, gCoupling, betaP and gamma

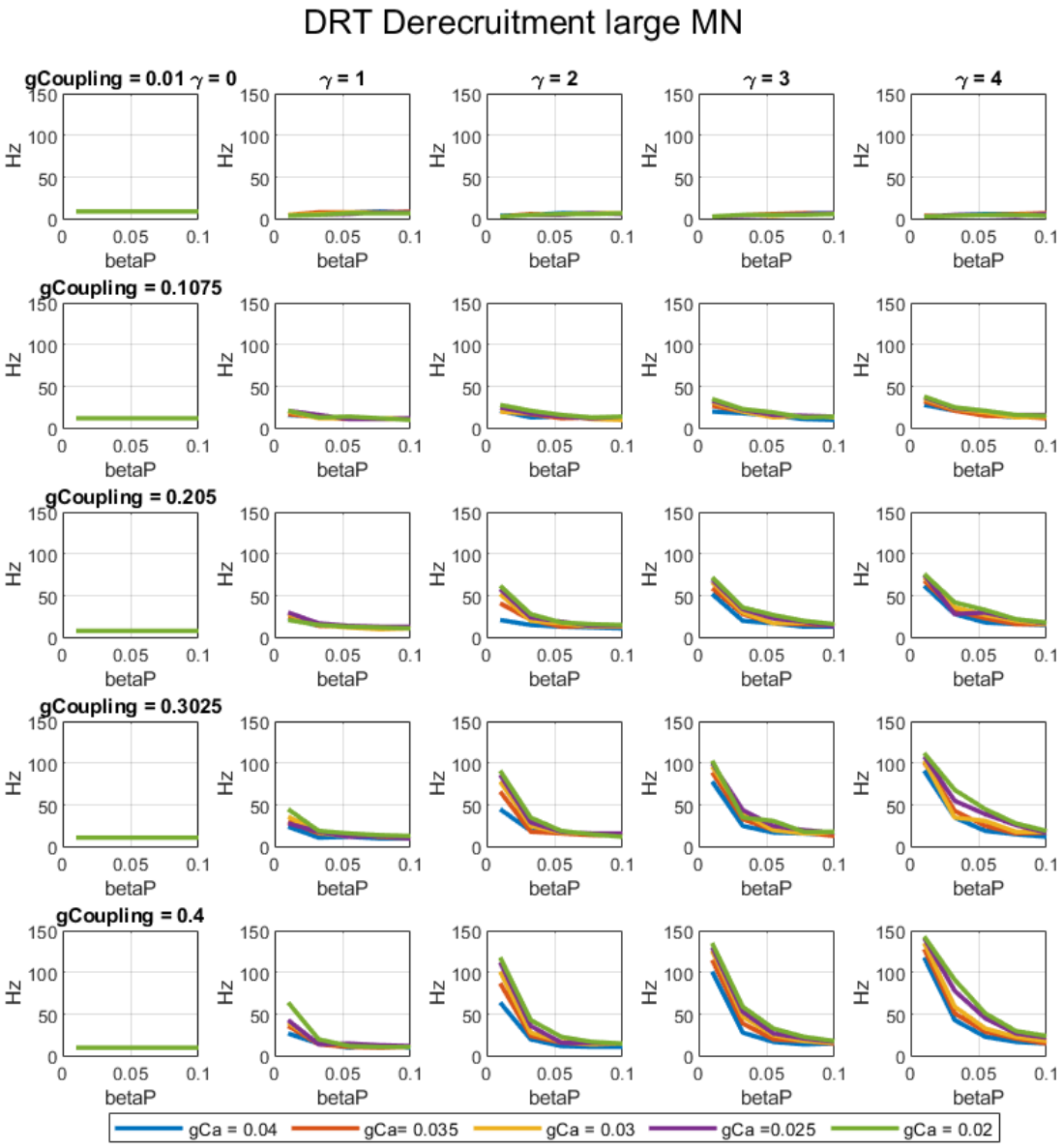

Figure 14: Modulation of the discharge rate at derecruitment for large motoneurons when changing gCa, gCoupling, betaP and gamma

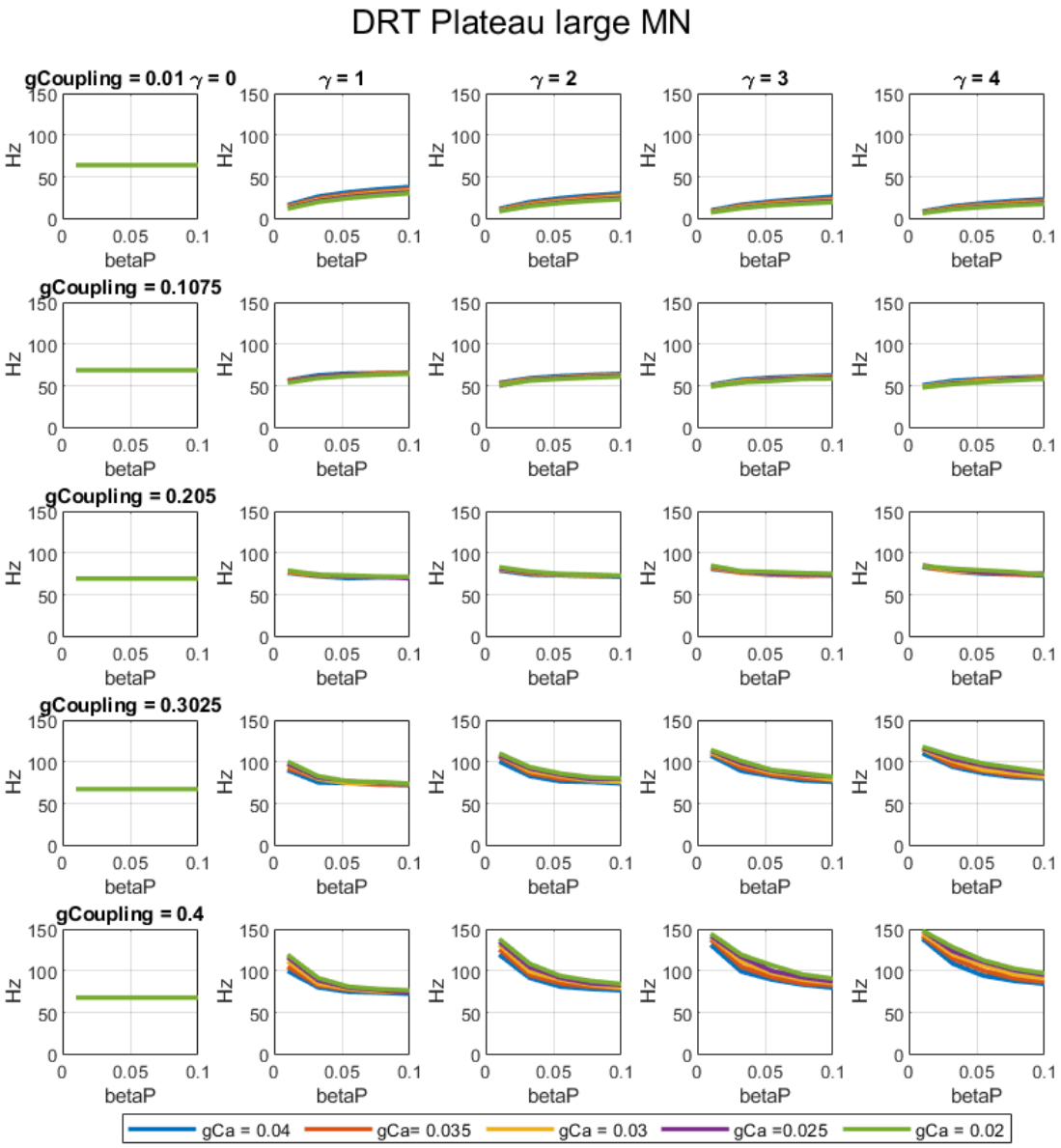

Figure 15: Modulation of the discharge rate at plateau for large motoneurons when changing gCa, gCoupling, betaP and gamma

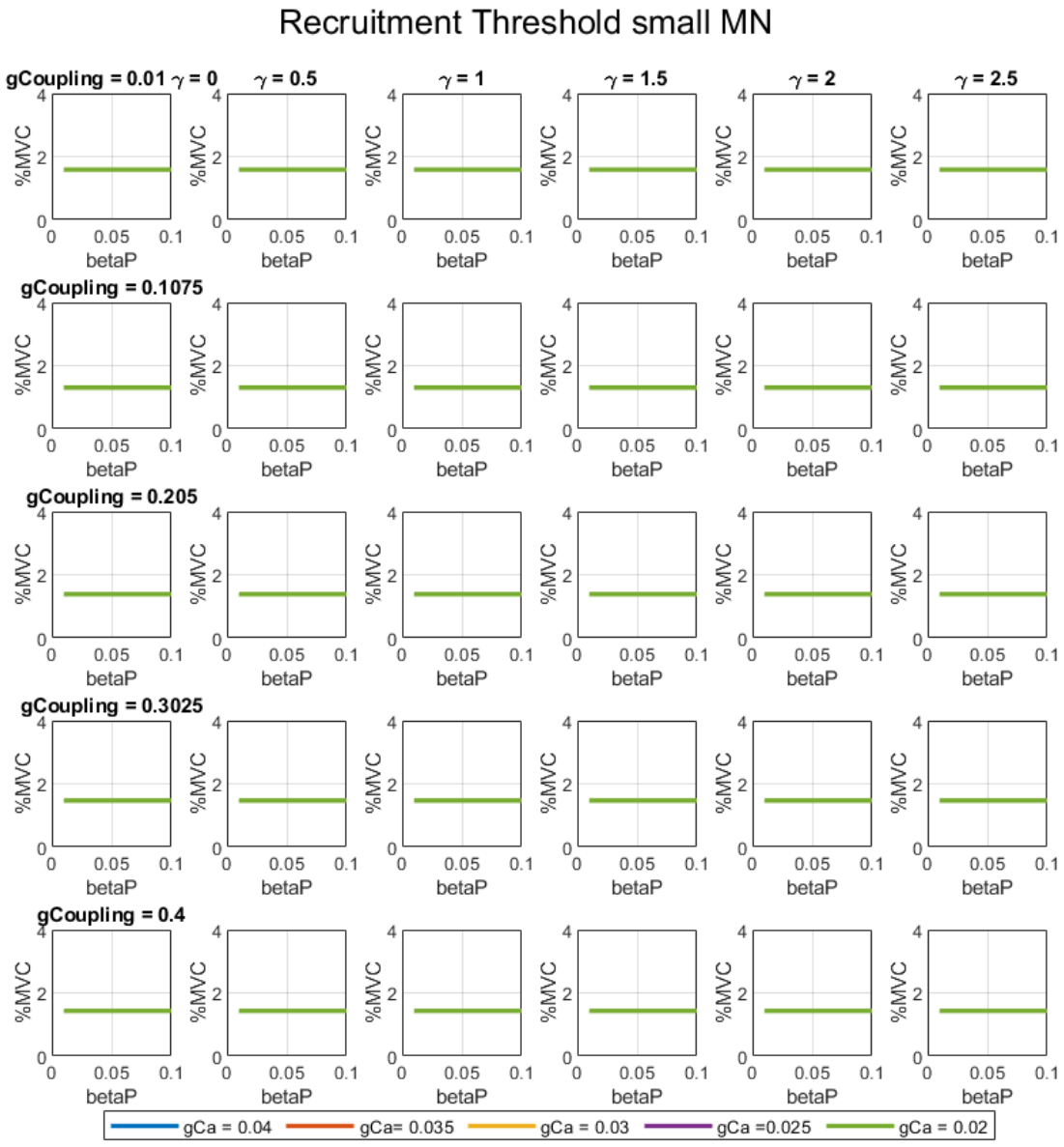

Figure 16: Modulation of the recruitment threshold for small motoneurons when changing gCa, gCoupling, betaP and gamma

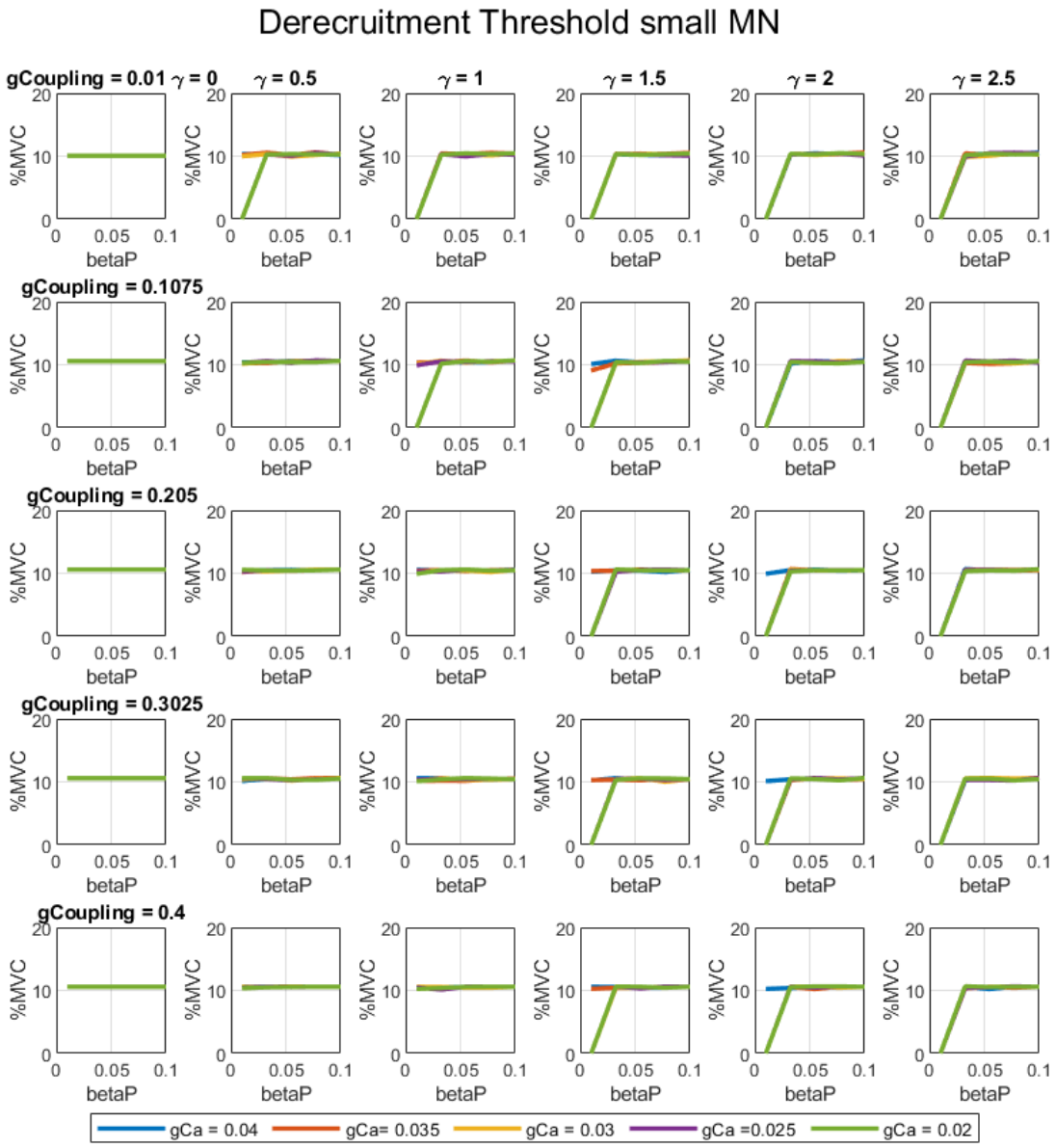

Figure 17: Modulation of the derecruitment threshold for small motoneurons when changing gCa, gCoupling, betaP and gamma

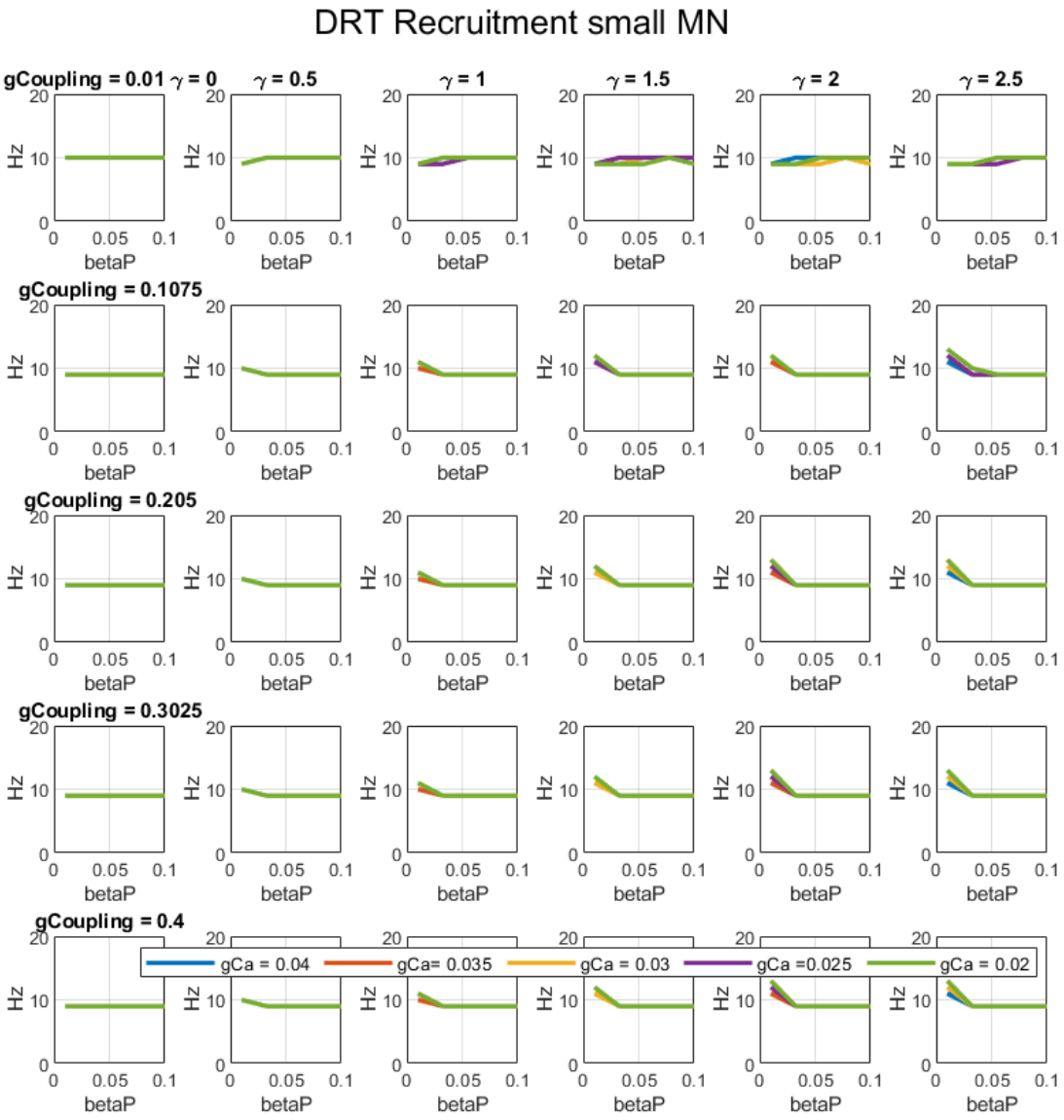

Figure 18: Modulation of the discharge rate at recruitment for small motoneurons when changing gCa, gCoupling, betaP and gamma

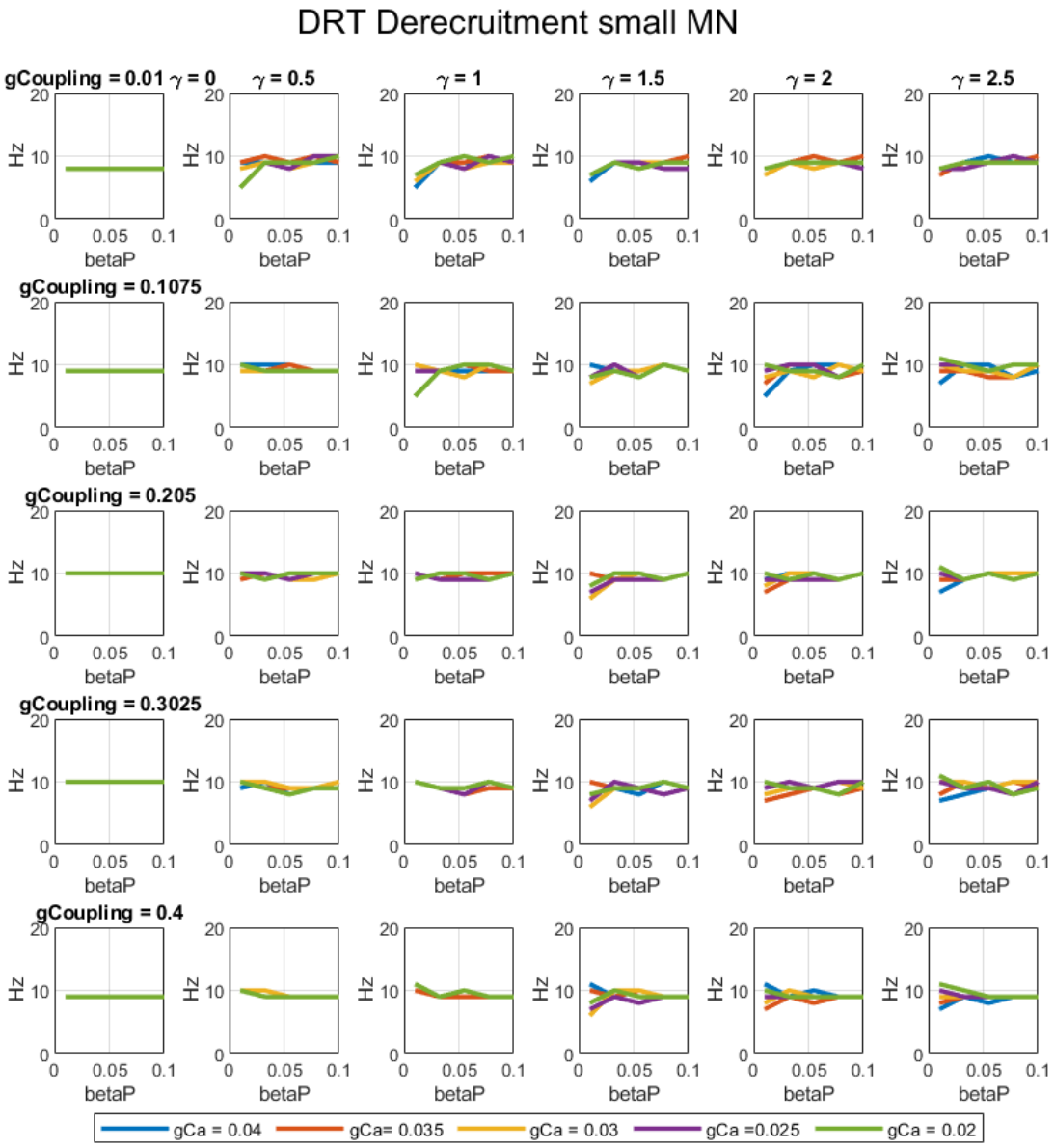

Figure 19: Modulation of the discharge rate at derecruitment for small motoneurons when changing gCa, gCoupling, betaP and gamma

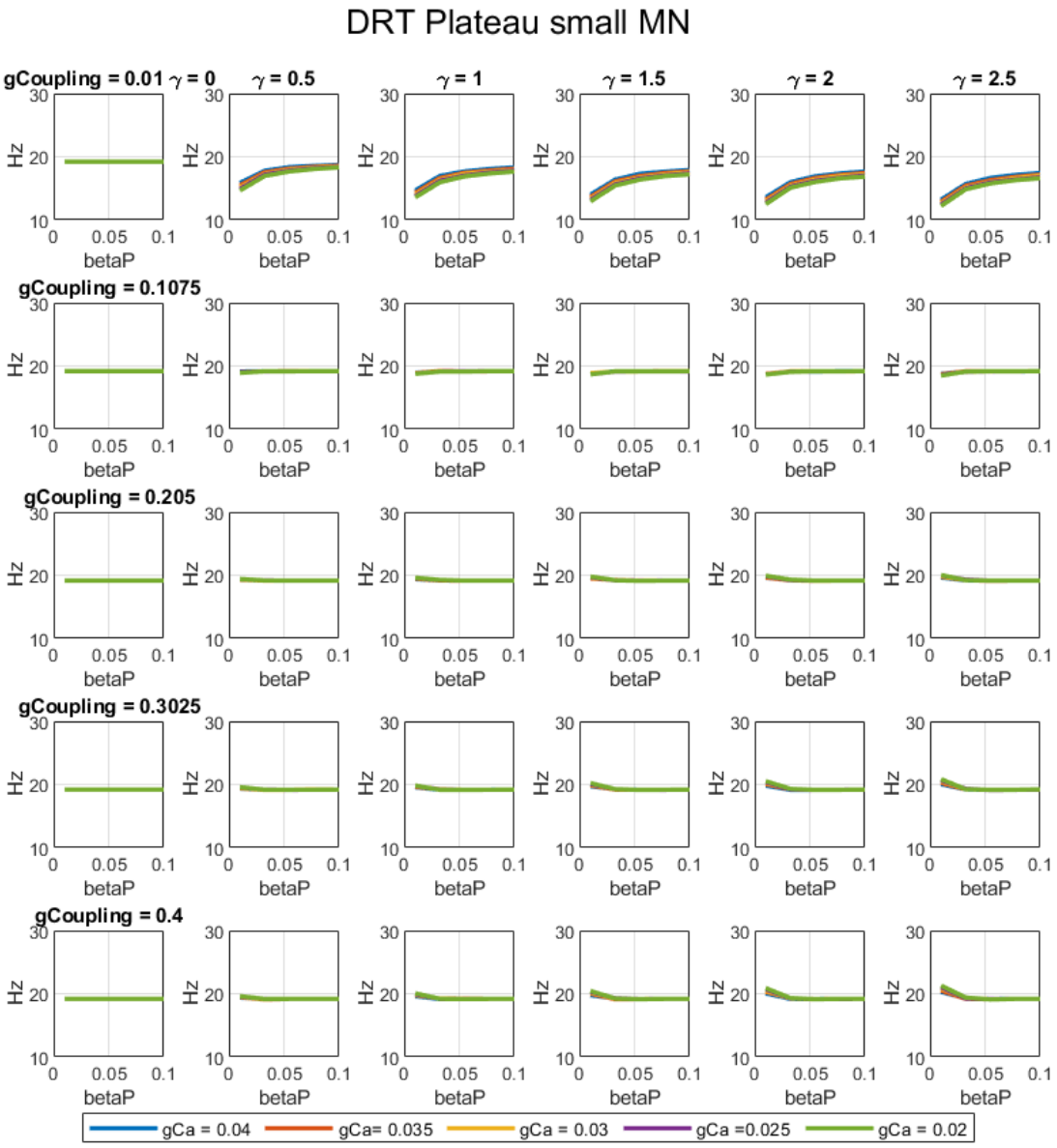

Figure 20: Modulation of the discharge rate at plateau for small motoneurons when changing gCa, gCoupling, betaP and gamma